

Classification of Precipitation Types in Lake-Effect Snow Events Using Dual-Polarimetric Doppler Radar Observations

Eric Ahasic, Jeffrey Frame, and Tim Cermak

Department of Atmospheric Sciences, University of Illinois at Urbana-Champaign, Urbana, IL

1. Introduction and Motivation

Every winter, metropolitan areas in the United States such as Cleveland, OH, Grand Rapids, MI, and Buffalo, NY, are impacted by lake-effect snowstorms. These snowstorms can result in feet of snow over only a few days, and can cripple metropolitan areas, or even entire regions. For an example, an early-season lake-effect event produced over three feet of snow in Buffalo, NY, during October 2006, damaging 90% of the city's trees (NWS Buffalo 2006). Other extreme lake-effect events include a 10-day event during February 2007, which resulted in over 100 inches of snow over the Tug Hill Plateau of Upstate New York (NCDC 2007), and an event that crippled Oswego, NY, for three days during January 2004 (NWS Buffalo 2009). Lake-effect snowfall is often localized, with a narrow band of heavy accumulations and nearby locations sometimes receiving little or no accumulation at all. As a result, accurate forecasts of snowfall amounts and coverage are necessary in order to have operations in place to cope with these events.

Past research has classified lake-effect snow storms into five primary categories (Niziol et al. 1995). The two most common of these are wind-parallel rolls, which generally result in a larger area of light accumulations and develop when the wind blows along the short axis of a lake, and long lake-axis-parallel, or shore-parallel bands that result in a smaller area of often heavier accumulation. Long lake-axis-parallel bands are more common over the Eastern Great Lakes (Ontario and Erie) than over the Western Great Lakes because the prevailing wind is directed along the major axis of these lakes during the cold season (Kristovich and Steve 1995). Past research on lake-effect events has generally focused on wind-parallel rolls as opposed to long-lake axis parallel bands (e.g., Braham 1990, Kristovich 1993).

In order to better understand long lake-axis-parallel lake effect events, an X-band, dual-polarization Doppler on Wheels (DOW) radar was utilized to observe these types of storms (Wurman 2001). The dual-polarization capabilities of the DOW allow for additional data to be collected on these events and subsequent hydrometeor classifications to be explored. While dual-polarization observations of warm-season convective storms have become more common in

recent years (e.g., Ryzhkov et al. 2005; Schuur et al. 2006; Frame et al. 2009), very few such studies have focused on cold season events, such as lake-effect snow. To date, no X-band dual-polarimetric observations of lake-effect snow bands exist.

A description of the methods used in this work, including background information on dual-polarization radar parameters, is discussed in section 2. Section 3 provides results taken from analysis of the radar data and surface hydrometeor observations. Conclusions and future work can be found in section 4.

2. Methods

Dual-polarization observations of long-lake axis parallel lake-effect snow bands over Lake Ontario were obtained using a Doppler on Wheels (DOW) radar during the winter of 2010-2011. Volume scans included radar reflectivity, radial velocity, and dual-polarization parameters such as differential reflectivity (Z_{DR}), specific differential phase (K_{DP}), and the correlation coefficient of horizontally polarized waves to vertically polarized waves (ρ_{hv}). Observations of surface weather conditions and hydrometeor types were taken at the radar location as well as at Oswego, NY, during selected deployments. By examining radar scans collected at the same time as the surface observations, potential relationships between hydrometeor types and dual-polarization radar parameters can be inferred.

Of the seven lake-effect cases on which data were collected during the winter of 2010-2011, four deployments were examined in detail, during which hydrometeor observations were taken. For the 4-5 January 2011 and 6 January 2011 cases, the DOW was stationed at Fair Haven, NY, on the south shore of Lake Ontario. For the 15 January 2011 and 10 February 2011 cases, the DOW was located just west of Oswego, NY, also on the shore of Lake Ontario (Fig. 1). Data from these deployments, as well as ones not explored in this work, were used in a companion study to relate dual-polarization fields to the presence of vortices and banded or cellular convection (Cermak et al. 2012).

Surface weather observations were collected at regular intervals, which varied depending on the deployment. Temperature, relative humidity, and wind speed and direction were measured, as well as the hydrometeor type and intensity if precipitation was occurring. Hydrometeor types included snow pellets, dendrites, or a combination of these. Unfortunately,

the radar beam was blocked over the city of Oswego from both the Fair Haven site and the site just west of Oswego, as shown in Figure 2. Thus, no useful radar data were collected directly over the surface observation site at Oswego. Furthermore, data within a 3 km radius of the DOW location suffered from a low signal-to-noise ratio. As a result, these data were of poor quality, prohibiting the direct comparison of simultaneous radar data and surface hydrometeor observations at either Oswego or the DOW site. Thus, it was necessary to examine data taken upstream from the surface observation site, and extrapolate it to the site based on the speed and direction of propagation of the radar echoes.

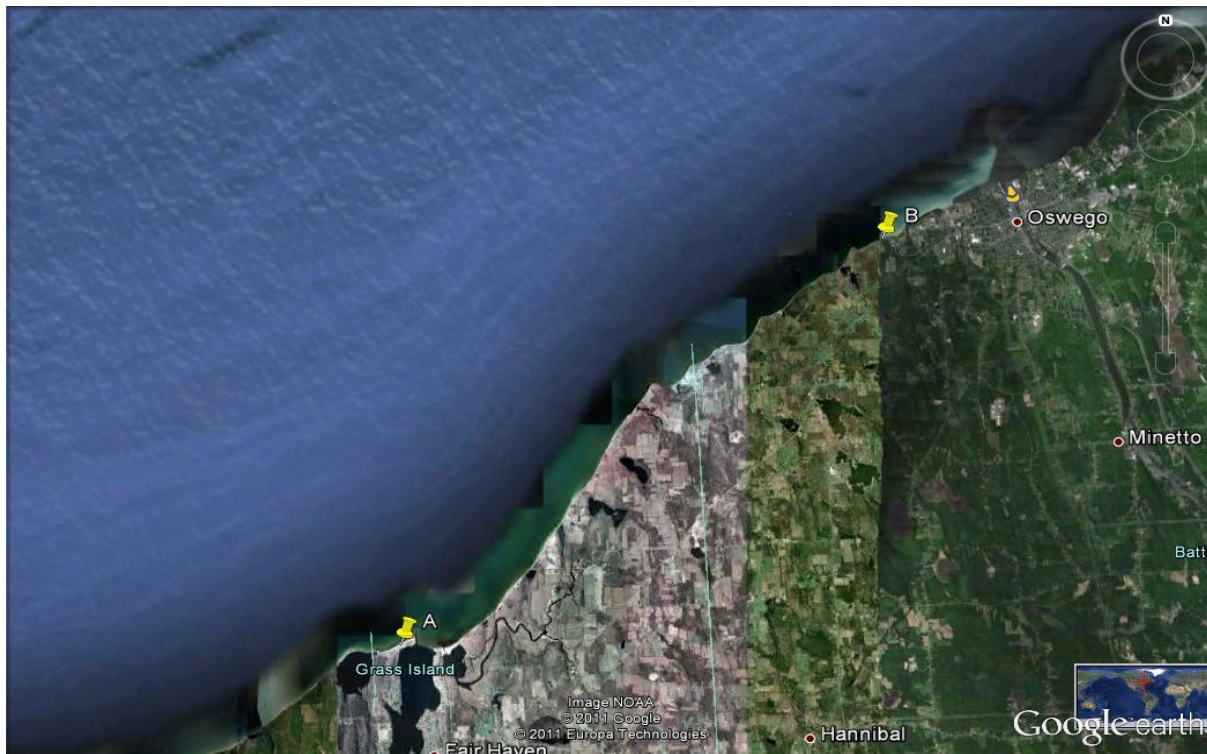


Figure 1: Map of DOW deployment sites along the shore of Lake Ontario. Point A corresponds to Fair Haven, NY, the radar deployment site for 4-5 January and 6 January. Point B corresponds to just west of Oswego, NY, the radar deployment site for 15 January and 10 February.

Analyzing and editing the data was done using SOLOII (Oye et al. 1995). Data with a low signal-to-noise ratio, as well as ground clutter and second trip echoes, were removed. An objective analysis was then performed on these data with REORDER software using Barnes (1964) weighting. An 8 km by 8 km was chosen to encompass the precipitation propagating towards the surface observation site. The Barnes weighting function, grid spacing, and radius of influence were selected in accordance with Pauley and Wu (1990) and Marquis et al. (2007). The

values selected depended on δ , the maximum observed data spacing in the analysis domain. This can be found from the equation $\delta = \theta R$, where θ is the beamwidth of the radar and R is distance between the radar and the farthest edge of the analysis domain. The beamwidth of the DOW was 0.93° and the value of R (which depended on the propagation speed of the precipitation) was 11 km for all deployments. The values for the horizontal grid spacing ($\Delta x = 3\delta$), radius of influence ($r_x = 5\delta / 12$) and the weighting function, $\kappa = (1.33\delta)^2$, were then calculated and can be found in Table 1.

θ (radians)	R (km)	δ (km)	r_x, r_y, r_z (km)	$\Delta x, \Delta y, \Delta z$ (km)	Weighting Function (κ)
0.0162 (0.93°)	11	0.1785	0.5356	0.0714	0.0564

Table 1: Values of the parameters used in the objective analysis of the radar data. Values for beamwidth (θ), distance between the radar and the farthest edge of the analysis domain (R), and maximum observed data spacing (δ) were constant for all deployments. The radii of influence (r_x, r_y, r_z), grid spacing ($\Delta x, \Delta y, \Delta z$), and weighting function (κ) were calculated as described in the text.

The objective analysis region depended on the speed and direction of the propagation of the precipitation. The objective analysis grid was centered upstream from the hydrometeor observation site over the radar echoes most likely to be located over the site at the time of the observation. This was accomplished by estimating the speed and direction of propagation of the radar echoes for each surface data collection time, which were nearly constant during a given deployment (Table 2). Examples of the objective analysis grid are shown in Figure 2.

Deployment	Grid Center (km from DOW)	Grid Length (km)	Grid Width (km)	Propagation Direction (degrees)	Propagation Speed (m/s)
January 4-5	8	8	8	280	7.7
January 6	8	8	8	285	8.2
January 15	8	8	8	270	7.7
February 10	8	8	8	270	9.3

Table 2: Size and location of the objective analysis grid for each deployment. Speed and direction of propagation of precipitation for each date were used to determine location of the grid. These values varied slightly between deployments but did not change during a deployment.

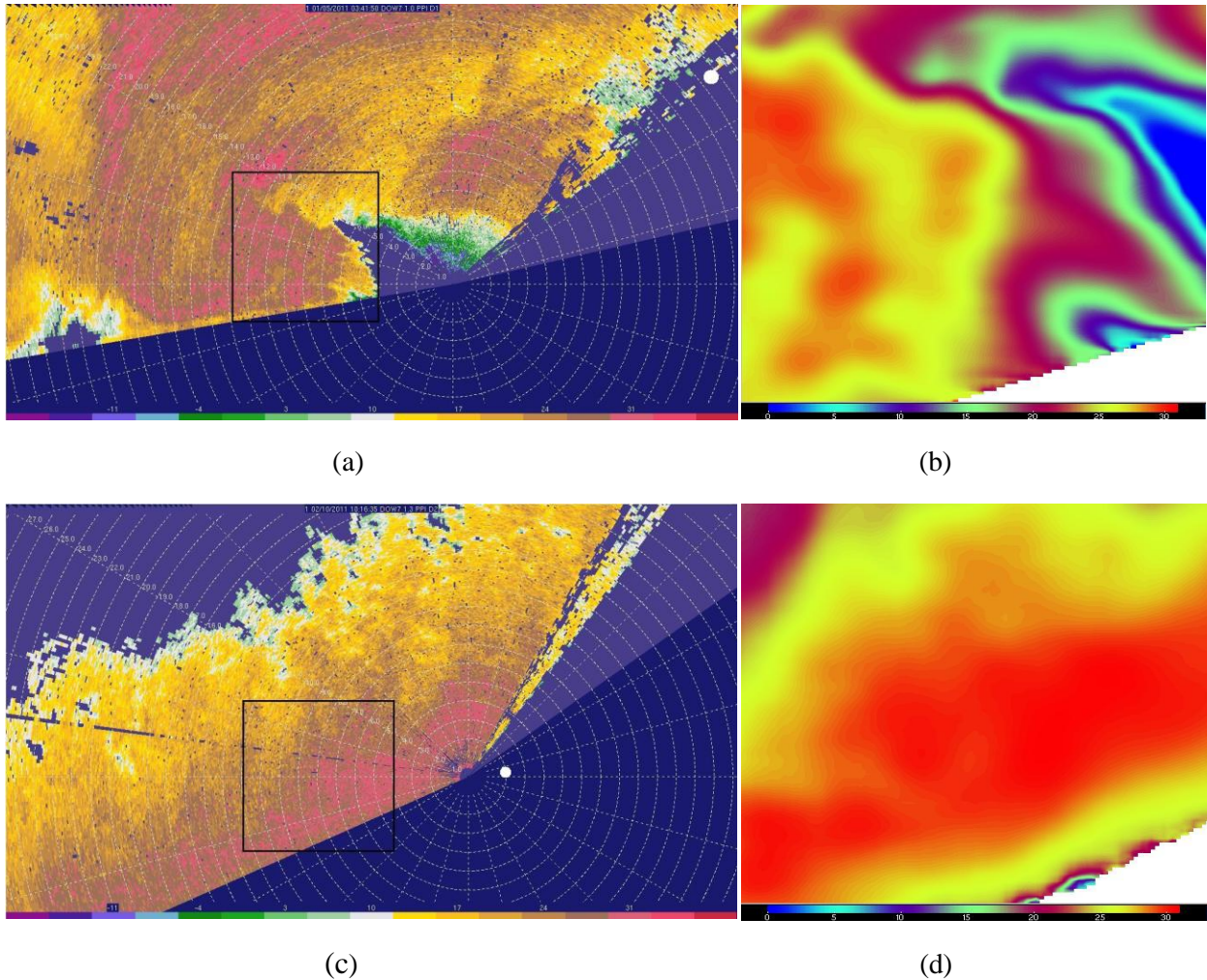


Figure 2: (a) Edited unanalyzed reflectivity from the 1° scan and (b) objectively analyzed reflectivity for 0345 UTC 5 January. (c) Edited unanalyzed reflectivity from the 1° scan and (d) objectively analyzed reflectivity for 1017 UTC 10 February. In (a) and (c), the black box represents the objective analysis domain, the white dot shows the location of the surface observation site at Oswego, range rings are plotted every 1 km, and azimuth angles are shown every 15 degrees. Elevation (AGL) for both objective analysis figures is 320m.

The DOW radar is dual-polarization radar, allowing for many more fields to be derived from the radar data than for a conventional Doppler radar. Differential reflectivity (Z_{DR}) can be calculated from the equation

$$Z_{DR} = 10\log_{10}(Z_{HH}/ Z_{VV})$$

where Z_{HH} is the horizontal reflectivity and Z_{VV} is the vertical reflectivity. For spherical hydrometeors, such as drizzle, the horizontal and vertical dimensions of the hydrometeors are roughly equal, meaning that the amount of horizontally and vertically scattered power should

also be roughly equal. Thus, the ratio between these is roughly one, so the logarithm is zero, leading to a Z_{DR} near zero for roughly spherical particles. Hydrometeors with their major axes oriented horizontally, such as falling raindrops and melting hail or graupel, generally have positive values for Z_{DR} because the horizontal reflectivity will be larger than the vertical reflectivity. Hydrometeors with their major axes oriented vertically, such as conical graupel, usually have negative values for Z_{DR} because the vertical reflectivity is greater than the horizontal reflectivity (Rinehart 2010, p. 211). Values of Z_{DR} for most ice particles are often near zero, as they do not have a preferred orientation while falling (Hall et al. 1984). Since a radar pulse volume of ice crystals usually contains a population of randomly oriented hydrometeors, the ratio of Z_{HH} and Z_{VV} for the pulse volume averages out to around one, and thus a Z_{DR} of zero (Hall et al. 1984). Ice may also exhibit lower values of Z_{DR} compared to liquid hydrometeors because ice has a lower complex index of refraction than water. Since the radar was calibrated using values of the complex index of refraction typical for liquid hydrometeors, ice particles of the same size often appear to have a lower Z_{HH} and Z_{VV} , and thus lower Z_{DR} (Houze 1993, p. 119).

Specific differential phase (K_{DP}) is the range derivative of the differential phase shift (Φ_{DP}), or the difference in the phase of the vertical and horizontally polarized pulses as a result of these waves passing through a particle (Ryzhkov and Znić 1995). K_{DP} can be calculated through the equation

$$K_{DP} = \Phi_{DP}(r_2) - \Phi_{DP}(r_1) / 2(r_2 - r_1)$$

in which r_1 and r_2 refer to two ranges from the radar (in km), such that $r_1 < r_2$ (Rinehart 2010, p. 214). Horizontally-oriented hydrometeors will produce an increasing, positive differential phase shift with range and thus a positive value for K_{DP} (Seliga and Bringi 1978). As a result, K_{DP} and Z_{DR} possess similar relationships to hydrometeor orientation, with horizontally-oriented hydrometeors generally returning positive values and vertically oriented particles exhibiting negative values. The magnitude of the differential phase shift is also related to the liquid water content in a pulse volume. For example, greater numbers of horizontally-oriented particles in a pulse volume lead to greater positive values for K_{DP} . This phase shift is greater for liquid hydrometeors than for ice. (Ryzhkov and Znić 1995).

The correlation coefficient between the returned horizontal and vertical power (ρ_{HV}) can be used to determine the consistency of hydrometeor types within a pulse volume. Mixed-phase hydrometeors, such as melting snow, typically possess relatively low values of ρ_{HV} (usually between 0.85-0.95). For pulse volumes consisting of hydrometeors of a consistent size and shape, values of ρ_{HV} will be approximately unity.

3. Results

The hydrometeors observed were classified into three primary types: Snow pellets, dendritic snowflakes, and mixtures of these (Table 3). Snow pellets generally form when supercooled water rimes onto a falling ice crystal, creating a somewhat spherical hydrometeor. Snow pellets contain pockets of air that become trapped as supercooled water freezes onto the pellet, lowering the density of the pellet below that of pure ice (Ahrens 2006, p. 182). Dendrites form differently than pellets, requiring colder temperatures and supersaturation with respect to water. Dendritic growth is most efficient around -15°C , at which the difference between the saturation vapor pressure over water and ice is greatest. Near this temperature, ice crystals grow rapidly into larger crystal structures, often in the form of dendrites or plates (Rogers and Yau 1989). Dendrites are even less dense than pellets as their structure contains many arms surrounded by air. The dendrites often collide with each other while falling and can accrete into clumps of dendrites, or else fall as single dendrites. Aggregation of dendrites is dependent on temperature, with the process being more efficient at warmer temperatures. Since dendrite formation does not require riming of supercooled water, they do not require temperatures in the cloud-bearing layer to be greater than -10°C .

The upper-air environment is depicted by rawinsonde data collected at Buffalo, NY (KBUF; Fig. 3). The sounding from 00 UTC 5 January shows temperatures greater than -10°C from just above the surface to 850 hPa. Since ice nuclei generally do not activate until the temperature is below -10°C , any cloud within this layer likely contained supercooled water. As ice crystals fell through this layer, they would have likely rimed with supercooled water and formed snow pellets. Table 3 indicates that pellets were observed more frequently on 5 January than on other date. Likewise, the sounding from 12 UTC 10 February shows that the temperature

of the entire atmospheric column was colder than -10°C , meaning that little or no supercooled water was likely present on this date. Dendrites were the main hydrometeor type observed on 10 February (Table 3), which is consistent with the above analysis. Since colder temperatures were observed on 10 February than on the other deployment dates, aggregation of dendrites into large clumps would have been less likely, and small dendrites would be expected. These findings are consistent with the data shown in Table 3.

Date	Time (UTC)	Temperature ($^{\circ}\text{C}$)	RH (%)	Wind Speed (kts)	Precipitation Type	Intensity
Jan 5	0115	-0.5	100	5.0	pellets	light
	0215	0	100	0.7	pellets, some dendrites	moderate
	0230	-0.5	100	2.3	pellets, pellet-like dendrites	moderate
	0300	-0.5	100	1.2	pellets	moderate
	0330	0	86	N/A	small pellets	light
	0345	-0.5	90	1.1	dendrite clumps, pellets	moderate
	0430	-0.5	96	4.4	dendrite clumps	heavy
	0500	-0.5	N/A	4.0	dendrite clumps	moderate
Jan 6	0445	-3.7	62	3.0	graupel	moderate
	0500	-3.6	60	1.0	dendrite and pellet mix	N/A
	0530	-4.5	71	3.0	larger dendrites	N/A
	0545	-4.6	85	3.0	dendrites and small pellets	moderate
Jan 15	0400	-0.9	87	4.0	dendrites and aggregates	light
	0530	-1.3	87	6.0	dendrites	moderate
	0545	-1.2	86	8.0	pellets	moderate
Feb 10	0737	N/A	N/A	N/A	small dendrites	light
	0954	N/A	N/A	N/A	small dendrites	moderate
	1017	N/A	N/A	N/A	small dendrites	heavy
	1052	-7.8	90	8.7	small and medium dendrites	heavy

Table 3: Surface observations taken during selected deployments. Observations on 5 Jan and 6 Jan were taken at Fair Haven, NY, while observations on 15 Jan and 10 Feb observations were taken just west of Oswego, NY.

Using the data in Table 3, relationships between the observed hydrometeor types and the dual-polarization parameters were inferred. Table 4 displays the various precipitation types (pellets, dendrites, or mixtures) and the associated values for the dual-polarization parameters. The values for the dual-polarization parameters in Table 4 were obtained subjectively from the objective analyses of the radar data. Ranges for the parameters are displayed, as opposed to single values, because each parameter varied throughout the analysis grid in most cases. For each

observation time, a single value was also subjectively identified that best represented the data in the analysis grid. This was accomplished by first selecting one value of reflectivity that best represented the precipitation in the grid which was estimated to be most likely to pass over the observation site after accounting for the precipitation propagation. Then, single representative values were also selected for the dual-polarization parameters from the same portion of the grid where the reflectivity value was taken. An example of this is shown in Figure 4. The mean of these representative values was found and also displayed in Table 4, to enable a general comparison of dual-polarization parameters between the various hydrometeor types.

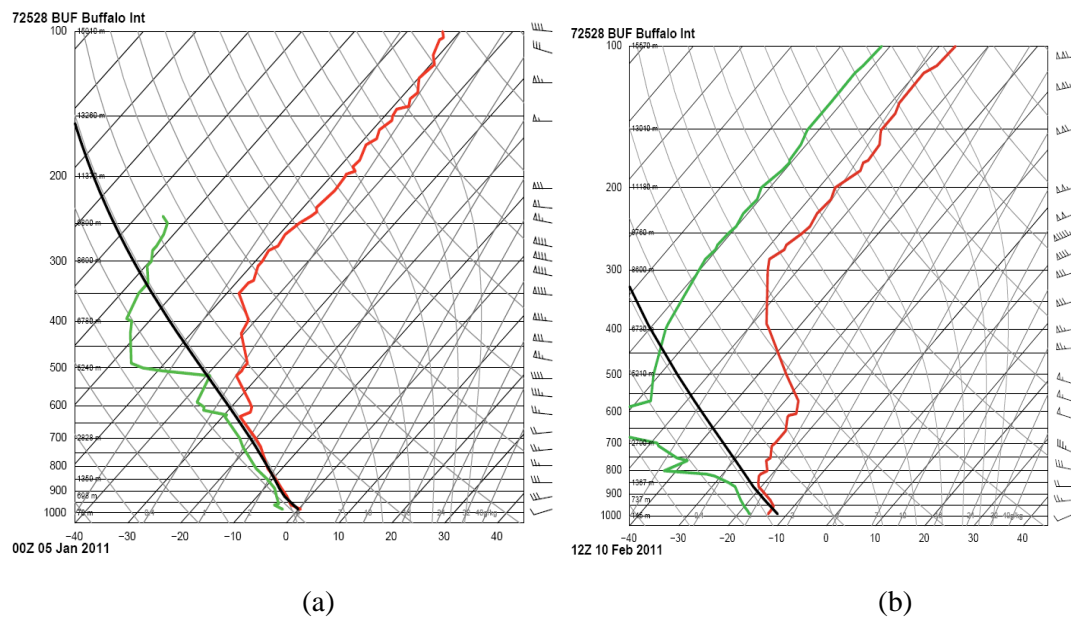


Figure 3: Soundings from Buffalo, NY (KBUF) for (a) 00 UTC 5 January and (b) 12 UTC 10 February. Pellets were primarily observed during the 5 January deployment, while dendrites were primarily observed during the 10 February deployment. The black line represents the temperature of an unmodified air parcel lifted from the surface. Soundings are courtesy of the University of Wyoming. (<http://weather.uwyo.edu/upperair/sounding.html>).

Relationships between hydrometeor type and Z_{DR} were explored by analyzing the values found in Table 4. Pellets showed the highest mean value for Z_{DR} , followed by mixtures of pellets and dendrites; dendrites exhibited the lowest mean value. This is consistent with the findings of Hall et al. (1984), in which lower density hydrometeors comprised of ice (such as dendrites) exhibited the lowest values of Z_{DR} , and roughly spherical hydrometeors of higher densities and also comprised of ice (pellets), exhibited higher values of Z_{DR} . The tumbling, non-preferred orientation of dendrites as they fall also result lower values of Z_{DR} for dendrites. Additionally, all

Z_{DR} values were positive for every observation time. It should also be noted that the radar calibration differed slightly among the 6 January, 5 January, and 10 February cases, especially as it relates to the dual-polarization parameters.

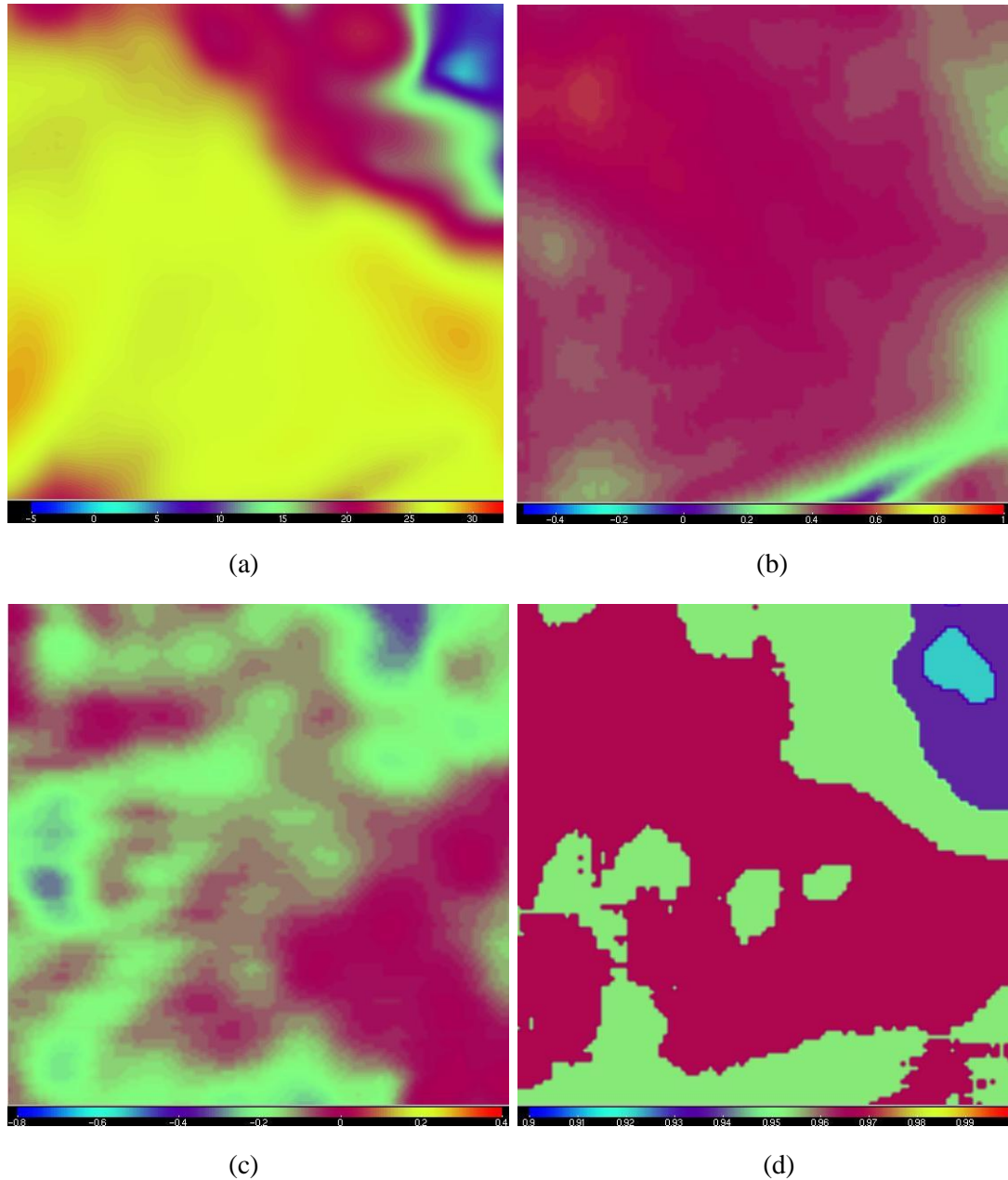


Figure 4: Objective analyses of (a) reflectivity, (b) Z_{DR} , (c) K_{DP} , and (d) ρ_{HV} from 0545 UTC 6 January. Representative values from Table 4 were selected by analyzing the reflectivity fields to find the regions of precipitation most likely to be over the observation site. Values of Z_{DR} , K_{DP} , and ρ_{HV} were then selected in this region. For example the representative values selected for this time were (a) 25 dbZ, (b) 0.5 dB, (c) -0.1 °/km, and (d) 0.97. Elevation (AGL) for objective analysis figures is 320m.

Table 4: Precipitation Observations and Values of Dual-Polarization Variables						
	Time/Date	Intensity	Reflectivity (dBZ)	Z_{DR} (dB)	K_{DP} (°/km)	ρ_{HV}
Pellets						
	01/05 0115 UTC	light	15-25 (15)	0.3-0.6 (0.5)	-0.3-(-0.1) (-0.2)	0.97-0.98 (0.97)
	01/05 0330 UTC	light	10-25 (20)	0.4-0.6 (0.5)	-0.3-0 (-0.1)	0.95-0.96 (0.95)
	01/05 0230 UTC	moderate	15-30 (25)	0.6-0.9 (0.8)	-0.3-0 (-0.2)	0.95-0.96 (0.95)
	01/05 0300 UTC	moderate	15-35 (25)	0.5-0.9 (0.8)	-0.2-0.1 (0.0)	0.95-0.97 (0.96)
	01/06 0445 UTC	moderate	10-25 (21)	0.5-0.8(0.7)	-0.2-0 (-0.1)	0.97-0.98 (0.98)
		Mean	21.0	0.66	-0.12	0.962
Dendrites						
	02/10 0737 UTC	light	15-25 (20)	0-0.2 (0.1)	-0.2-0 (-0.1)	>0.98 (0.98)
	02/10 0954 UTC	moderate	20-30 (30)	0.2-0.5 (0.3)	-0.2-0 (-0.1)	0.96-0.97 (0.97)
	01/05 0500 UTC	moderate	20-35 (25)	0.5-0.7 (0.6)	-0.3-0 (-0.2)	0.97-0.98 (0.98)
	01/05 0430 UTC	heavy	15-25 (25)	0.4-0.6 (0.5)	-0.3-(-0.1) (-0.2)	>0.98 (0.99)
	02/10 1017 UTC	heavy	25-35 (30)	0.3-0.6 (0.5)	-0.2-0.1 (0.0)	>0.98 (0.99)
	02/10 1052 UTC	heavy	15-25 (20)	0.1-0.3 (0.2)	-0.2-0 (-0.1)	>0.98 (0.99)
	01/06 0530 UTC	N/A	15-25 (20)	0-0.3 (0.1)	-0.2-0 (-0.1)	0.96-0.97 (0.97)
		Mean	24.3	0.33	-0.11	0.981
Dendrites and Pellets						
	01/05 0215 UTC	moderate	15-30 (20)	0.6-0.9 (0.8)	-0.3-0 (-0.2)	0.95-0.96 (0.95)
	01/05 0345 UTC	moderate	15-30 (25)	0.4-0.7 (0.5)	-0.2-0 (-0.1)	0.95-0.97 (0.96)
	01/06 0545 UTC	moderate	20-30 (25)	0.4-0.6 (0.5)	-0.2-0 (-0.1)	0.96-0.97 (0.97)
	01/06 0500 UTC	N/A	15-25 (20)	0-0.3 (0.1)	-0.2-0 (-0.1)	0.96-0.97 (0.96)
		Mean	22.5	0.48	-0.13	0.96

Table 4: Observations of dual-polarization parameters for selected deployments. Values were taken subjectively from the objective analyses of the radar data. A range of values is given for each parameter, as well as a representative value (bold). Mean values for each parameter were found by taking the mean of these representative values.

A more direct relationship can be found between the correlation coefficient (ρ_{HV}) and the various hydrometeor types. Since ρ_{HV} is related to the consistency of hydrometeors in a pulse volume, radar data taken when only pellets or only dendrites were occurring should exhibit higher ρ_{HV} values than data taken for mixed hydrometeor types. This is evident in Table 4, with dendrites generally displaying the highest values for ρ_{HV} , followed by snow pellets. This was expected as the dendrites were of similar composition and hydrometeor type. Mixtures of dendrites and pellets exhibited the lowest values, also as expected. Pellets exhibited low values of ρ_{HV} similar to those found for mixtures of pellets and dendrites because multiple phases of water must be present for pellet formation. Additionally, a relationship between ρ_{HV} and precipitation intensity may also be present because ρ_{HV} values are closer to unity when pellets or

dendrites were falling at a heavy intensity than when they were falling with a moderate or light intensity.

While specific differential phase (K_{DP}) was also analyzed, no potential relationship with hydrometeor type was able to be found. Since values of Z_{DR} for pellets, dendrites and mixtures of these are all positive, it can be assumed that these hydrometeors generally possess at least a slight horizontal orientation. For horizontally-oriented hydrometeors, K_{DP} is also expected to be positive. However, K_{DP} values often were negative, which is inconsistent with the values for Z_{DR} . Additionally, the K_{DP} data were noisy and the objective analysis was unable to remove much of this variability (e.g., Fig. 5). The K_{DP} fields were similar to these for many of the volume scans analyzed, making defining any range of K_{DP} values, or a representative value, difficult. As a result, no definitive relationship between K_{DP} and the hydrometeor type could be determined from the data available.

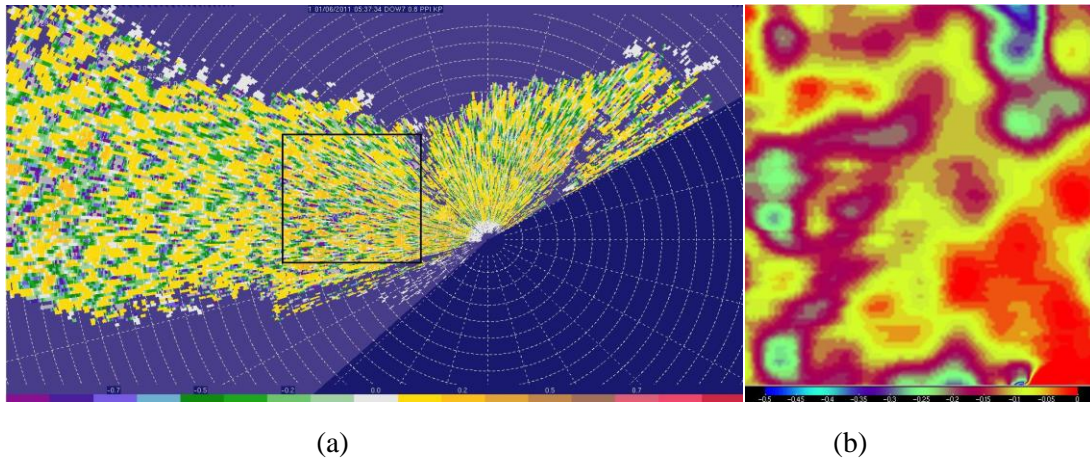


Figure 5: (a) Edited unanalyzed KDP from the 1° scan and (b) objective analysis of K_{DP} for 0545 UTC 6 January. The black box on the SOLOII image (a) represents the objective analysis domain overlaid on the raw K_{DP} data. Range rings are plotted every 1 km and azimuth shown every 15 degrees. Elevation (AGL) for objective analysis figure is 320m.

4. Conclusions and Future Work

Initial results indicate that potential relationships exist between hydrometeor types and dual-polarization parameters for lake-effect snow events. Through objective analysis of the radar data, a relationship between Z_{DR} and hydrometeor type was evident, with snow pellets returning higher values of Z_{DR} than dendritic snowflakes. This agrees with findings from past studies,

which showed dendrites having lower values for Z_{DR} than pellets. Values of Z_{DR} for mixtures of snow pellets and dendrites fell between the values for dendrites and pellets. Dendrites also exhibited higher values of ρ_{HV} compared to snow pellets and mixtures of both; also of note is how the values for ρ_{HV} were similar for snow pellets and dendrite and pellet mixtures. While K_{DP} appeared to be unreliable for the deployments studied, and thus no definitive relationship could be determined, this merits further investigation in future field studies.

While the bulk of dual-polarization research on hydrometeor classifications has focused on warm-season convective events, there is still much to explore for lake-effect snow and other cold season precipitation events. Future field experiments similar to this one would allow for more data to be collected and analyzed. While this study examined only X-band dual-polarimetric radar observations of long lake axis-parallel lake-effect snow bands over Lake Ontario, these are not necessarily representative of all lake-effect snow events. Further research could examine different lake-effect snow band types or lake-effect snow bands over other regions, within different atmospheric environments, and of varying intensities. Similar approaches can be utilized in examining other cold-season precipitation events using X-band dual-polarimetric radar observations as well. If ranges of values for dual-polarization parameters from any such projects are similar to the ones found in this work, an X-band hydrometeor classification using dual-polarization parameters may be possible for lake-effect snow or other cold-season precipitation events. Additional research using S-band or K-band dual-polarization radars may also add more insight into cold-season dual-polarization hydrometeor classification. As the National Weather service's WSR-88D radars become upgraded to dual-polarization capabilities, using them to explore hydrometeor classifications of lake-effect snow would be of great use to operational forecasters. Such classifications could be of great value operationally for forecasting snowfall totals or precipitation intensities and types from these storms.

Acknowledgements. We are grateful to Dr. Scott Steiger of the State University of New York at Oswego for his assistance with this project and all of the volunteers (too numerous to mention) who helped with the data collection. We also thank Dr. Josh Wurman, Dr. Karen Kosiba, and Justin Walker of the Center for Severe Research for operating the DOW radar and David Wojtowicz of the University of Illinois at Urbana-Champaign for technical assistance. Support from NSF Grant No. AGS10-42854 is also acknowledged.

5. References

- Ahrens, C. D., 2006: *Meteorology Today*. Brooks Cole, 549 p.
- Barnes, S. L., 1964: A technique for maximizing details in numerical weather map analysis. *J. Appl. Meteor.*, **3**, 396–409.
- Braham, R. R., Jr., 1990: Snow particle size spectra in lake-effect snows. *J. Appl. Meteor.*, **29**, 200-207.
- Cermak, T., J. Frame, and E. Ahasic, 2012: Dual-polarization observations of vortices and cellular convection within lake-effect snow bands. Preprints, *16th Symposium on Meteorological Observation and Instrumentation*, New Orleans, LA, Amer. Meteor. Soc., paper 6.6.
- Frame, J., P. Markowski, Y. Richardson, J. Straka, J. Wurman, 2009: Polarimetric and dual-Doppler radar observations of the Lipscomb County, Texas, supercell thunderstorm on 23 May 2002. *Mon. Wea. Rev.*, **137**, 544–561.
- Hall, M., J. Goddard, and S. Cherry, 1984: Identification of hydrometeors and other targets by dual-polarization radar. *Radio Sci.*, **19**, 132-140.
- Houze, R. A., 1993: *Cloud Dynamics*. Academic, 119 pp.
- Kristovich, D. A. R., 1993: Mean circulations of boundary-layer rolls in lake-effect snow storms. *Bound.-Layer. Meteor.*, **63**, 293-315.
- Kristovich, D. A. R., and R. A. Steve, III, 1995: A satellite study of cloud-band frequencies over the Great Lakes. *J. Appl. Meteor.*, **34**, 2083-2090.
- Marquis, J. N., Y. P. Richardson, J. M. Wurman, 2007: Kinematic observations of misocyclones along boundaries during IHOP. *Mon. Wea. Rev.*, **135**, 1749–1768.
- National Climatic Data Center, 2007: Climate of 2007 - February in historical perspective. [Available online at <http://www.ncdc.noaa.gov/oa/climate/research/2007/feb/feb07.html>.]
- National Weather Service Forecast Office, Buffalo, NY, 2006: Historic lake effect snow storm of October 12-13, 2006. [Available online at <http://www.erh.noaa.gov/buf/storm101206.html>.]
- National Weather Service Forecast Office, Buffalo, NY, 2004: Lake effect storm Iron. [Available online at <http://www.erh.noaa.gov/buf/lakeeffect/lake0304/i/stormi.html>.]
- Niziol, T. A., W. R. Snyder, and J. S. Waldstreicher, 1995: Winter weather forecasting throughout the Eastern United States. Part IV: Lake effect snow. *Wea. Forecasting*, **10**, 61–77.
- Oye, R., C. Mueller, and S. Smith, 1995: Software for radar translation, visualization, editing, and interpolation. Preprints, *27th AMS Conf. on Radar Meteorology*, Vail, CO, Amer. Meteor. Soc., 1995.

- Pauley, P. M., X. Wu, 1990: The theoretical, discrete, and actual response of the Barnes objective analysis scheme for one- and two-dimensional fields. *Mon. Wea. Rev.*, **118**, 1145–1164.
- Rinehart R. E., 2010: *Radar for Meteorologists*. Rinehart Publications, 482 pg.
- Rogers, R. R., and M. K. Yau, 1989: *A Short Course in Cloud Physics*. Butterworth Heinemann, 290 pg.
- Ryzhkov, A. V., T. J. Schuur, D. W. Burgess, P. L. Heinselman, S. E. Giangrande, and D. S. Zrnic, 2005: The Joint Polarization Experiment. *Bull. Amer. Meteor. Soc.*, **86**, 809–824.
- Ryzhkov, A. V., D. S. Zrnić, 1995: Comparison of dual-polarization radar estimators of rain. *J. Atmos. Oceanic Technol.*, **12**, 249–256.
- Schuur, T. J., A. V. Ryzhkov, and S. E. Giangrande, 2006: Winter precipitation type classification with a polarimetric WSR-88D radar. Preprints, *12th Conf. on Aviation, Range, and Aerospace Meteor.*, Atlanta, GA, Amer. Meteor. Soc., available online at http://ams.confex.com/ams/Annual2006/techprogram/paper_104497.htm.
- Seliga, T. A., and V. N. Bringi (1978), Differential reflectivity and differential phase shift: Applications in radar meteorology, *Radio Sci.*, 13(2), 271–275.
- Wurman, J. M., 2001: The DOW Multiple-Doppler Network. Preprints, *30th Int. Conf. on Radar Meteorology*, Munich, Germany, Amer. Meteor. Soc., 95-97.